

ENERGETICS AND PARTITION FUNCTION OF H₃⁺ MOLECULAR ION

ILKKA KYLÄNPÄÄ¹ AND TAPIO T. RANTALA²

Department of Physics, Tampere University of Technology, P.O. Box 692, FI-33101 Tampere, Finland

Submitted to The Astrophysical Journal

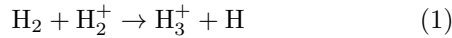
ABSTRACT

Full *NVT* quantum statistics of the H₃⁺ ion is simulated at low densities using the path integral Monte Carlo approach. For the first time, the molecular total energy, partition function, free energy, entropy and heat capacity are evaluated in temperatures relevant for planetary atmospheric physics. Temperature and density dependent dissociation recombination reaction balance of the molecule and its fragments above 4000 K is described, and also, the density dependence of thermal ionization above 10000 K is demonstrated. We introduce a new well-behaving analytical model for the molecular partition function of the H₃⁺ ion for the temperature range below dissociation and fit the parameters to the energetics from our simulations. The approach presented here can be regarded as an extension of the traditional *ab initio* quantum chemistry beyond the Born–Oppenheimer approximation to description of nonadiabatic phenomena, and even further, account of nuclear quantum dynamics.

Subject headings: molecular data – stars: atmospheres

1. INTRODUCTION

The H₃⁺ molecular ion has been a subject of a number of theoretical and experimental studies since its first experimental detection (Thomson 1911). Because of its rapid formation through the exothermic reaction ($\Delta E \approx -1.7$ eV)



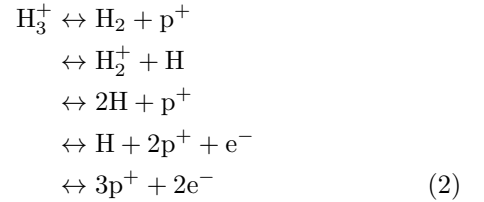
the H₃⁺ ion is expected in any active environment containing molecular hydrogen (Neale and Tennyson 1995), and thus, it is encountered, e.g. in the studies of the giant planets (Lystrup *et al.* 2008; Koskinen *et al.* 2009).

In planetary atmospheric physics, importance of the H₃⁺ ion lies in its capability to act as a cooling agent via infrared radiation (Neale *et al.* 1996; Harris *et al.* 2004; Koskinen *et al.* 2007). The atmospheric models taking into account this cooling are commonly based on the high temperature molecular partition function of the H₃⁺ ion (Neale and Tennyson 1995). Evaluation of the partition function faces, however, a few challenges of which the first one is finding a good approximation to the infinite summation over all rovibrational quantum states with accurate enough energies (Neale and Tennyson 1995). This has usually been worked out with calculations of a finite number of states from, e.g. a semi-empirical potential energy surface (Dinelli *et al.* 1995).

The next challenge comes with the changing geometry of the H₃⁺ ion at finite temperature. The rovibrational model needs to be extended for calculations of correct energetics for the emerging linear geometry of the weakly bound molecule (Neale *et al.* 1996).

Finally, at about the same temperature, where linear geometries start contributing, the molecule may also dis-

sociate to its fragments, and in fact, the equilibrium



needs to be considered above about 4000 K, the balance depending strongly on both the temperature and the density.

This brings forth two questions, at the least. First, how relevant it is to consider the molecular energetics and related partition function at temperatures where the molecule has dissociated and appears in form of fragments of the equilibrium reaction, Eq. (2), only. Secondly, the balance of the equilibrium reaction may be strongly affected, not only by the density, but also by the environment including the neutralizing negative counterparts of the positive H₃⁺. Thus, the thermal dissociation–recombination balance above about 4000 K gives rise to problems, which have not been taken into account in this context, yet.

In this study, using the path integral quantum Monte Carlo (PIMC) method we have carried out the first simulations of the full quantum statistics of the H₃⁺ ion, described by Eq. (2), at low densities and high temperatures ranging from 160 K up to about 15000 K. PIMC is the method to meet the above challenges: we need not make any approximations or restrictions in the summing over states, geometries or quantum description of dynamics. The finite temperature is inherent in the PIMC approach and the Coulomb many-body treatment of the particle interactions is exact. The PIMC method is computationally expensive, but feasible for small enough systems. (Ceperley 1995; Pierce and Manousakis 1999; Kwon and Whaley 1999; Knoll and Marx 2000; Cuervo and Roy 2006; Kylänpää and Rantala 2009).

The conventional quantum chemical *ab initio* descrip-

¹ email: ilkka.kylanpaa@tut.fi

² email: Tapio.Rantala@tut.fi

tion of the H_3^+ ion emerges as the zero Kelvin extrapolate from the PIMC simulations as we have shown earlier (Kylänpää and Rantala 2010). There, we evaluated the differences between three models for the description of the nuclear dynamics: Born–Oppenheimer approximation, nuclei in thermal motion and nuclei with both thermal and quantum dynamics. At low temperatures the necessity of the fully quantum mechanical approach for all five particles was established.

In the next section we present the essential details of the Feynman path integral quantum statistical approach, numerical simulation method and the model of the H_3^+ ion. In section 3 we present and analyze the energetics, partition function and other thermodynamic functions of the system using analytical forms where pertinent. In the last section the conclusions are given.

2. METHOD AND MODELS

According to the Feynman path integral formulation of the quantum statistical mechanics (Feynman 1998) the partition function of interacting distinguishable particles is given by the trace of the density matrix $\hat{\rho}(\beta) = e^{-\beta\hat{H}}$ as

$$Z = \text{Tr} \hat{\rho}(\beta) = \int dR_0 dR_1 \dots dR_{M-1} \prod_{i=0}^{M-1} e^{-S(R_i, R_{i+1}; \tau)},$$

where the action $S(R_i, R_{i+1}; \tau)$ is taken over the path $R_i \rightarrow R_{i+1}$ in imaginary time $\tau = \beta/M$, where $\beta = 1/k_B T$ and M is called the Trotter number. The trace implies a closed path ($R_M = R_0$).

For simulation we use the pair approximation in the action (Storer 1968; Ceperley 1995) for the Coulomb interaction of charges. This is exact in the limit $M \rightarrow \infty$, however, chemical accuracy is reached with sufficiently large M , i.e. small enough τ . Sampling in the configuration space $\{R_i\}_i^\infty$ in NVT ensemble is carried out using the Metropolis algorithm (Metropolis *et al.* 1953) with bisection moves and displacement moves (Chakravarty *et al.* 1998). The total energy is calculated using the virial estimator (Herman *et al.* 1982).

The error estimate in the PIMC scheme is commonly given in powers of the imaginary time time-step τ (Ceperley 1995). Therefore, in order to systematically determine the thermal effects on the system we have carried out all the simulations with $\tau = 0.03 E_H^{-1}$, where E_H denotes the unit of Hartree. Thus, the temperatures and the Trotter number M are related by $T = (k_B M \tau)^{-1}$, where k_B is the Boltzmann constant.

In the following we mainly use the atomic units, where the lengths, energies and masses are given in the units of Bohr radius (a_0), Hartree (E_H) and free electron mass (m_e), respectively. Thus, for the mass of the electrons we take $m_e = 1$ and for the protons $m_p = 1.83615267248 \times 10^3 m_e$. Conversion of the units of energy is given by $E_H = 219474.6313705 \text{ cm}^{-1} \approx 27.2 \text{ eV}$, and correspondingly, $k_B = 3.1668152 \times 10^{-6} E_H \text{ K}^{-1}$.

The statistical standard error of the mean (SEM) with 2 SEM limits is used as an error estimate for the evaluated observables.

For the NVT simulations we place one H_3^+ ion, i.e. three protons and two electrons, into a cubic box and apply periodic boundary conditions and the minimum

image principle. The simulations are performed in three different super cell (box) volumes: $(300a_0)^3$, $(100a_0)^3$ and $(50a_0)^3$. These correspond to the mass densities of $\sim 1.255 \times 10^{-6} \text{ g cm}^{-3}$, $\sim 3.388 \times 10^{-5} \text{ g cm}^{-3}$ and $\sim 2.710 \times 10^{-4} \text{ g cm}^{-3}$, respectively. The density has no essential effect at low T , where dissociation rarely takes place. At higher T , however, the finite density gives rise to the molecular recombination balancing the more frequent dissociation.

It should be pointed out that application of the minimum image principle with only one molecular ion in the periodic super cell may both give rise to the finite-size effects and also disregard higher density distribution effects, i.e. fragments of several ions in the simulation box. Thus, the lower the density the better we minimize the finite-size effects, which in this work are negligible, if not absent. The zero density limit cannot be reached due to the finite T . To avoid all these ambiguities we define our targets as molecular energetics, molecular partition function and other related molecular quantities. Therefore, in the following, we also exclude the trivial contribution from the center-of-mass thermal dynamics and energy $\frac{3}{2} k_B T$ to the molecular quantities.

The nuclear quantum dynamics, which was shown to be essential at low T , turns out to be negligible at higher temperatures. It is included, however, to be consistent with the low temperature results and our earlier study. For more details about the model and a discussion about the here neglected contribution from the exchange interaction see Kylänpää and Rantala (2010).

3. RESULTS AND DISCUSSION

3.1. Overview of molecular energetics

In Fig. 1 the NVT total energy (canonical ensemble internal energy) of the H_3^+ ion and its fragments is shown as a function of temperature. The molecular energy does not include the center-of-mass translational kinetic energy $\frac{3}{2} k_B T$. The data from simulations are given as circles, squares and triangles corresponding to the three densities. The PIMC data is also given in Tables 1 and 2.

The solid lines at $T < 4000 \text{ K}$ are fitted to analytical model forms but at higher temperatures lines are for guiding the eye, only. Our low temperature fit and analytical model, Eq. (7), is given as a blue dashed line and is discussed in the next sections in more detail. For comparison the energies from the fitted partition function of Neale and Tennyson (1995) is shown as black dots. These two do not manifest dissociation, and therefore, are not relevant at "higher T ".

The horizontal dash-dotted lines show the zero Kelvin energies for the ion and its fragments in Eq.(2). One of these lines presents the energy for the "barrier to linearity", i.e. the energy needed for the transformation to linear molecular geometry. It is also seen to be roughly the barrier to dissociation within the considered molecular densities.

Above 4000 K the density dependence is clearly seen as varying composition of fragments. In the range from 4000 to 10000 K the changing dissociation recombination balance leads to distinctly different energetics, and above that, at our highest simulation temperatures the thermal ionization of hydrogen atoms starts contributing

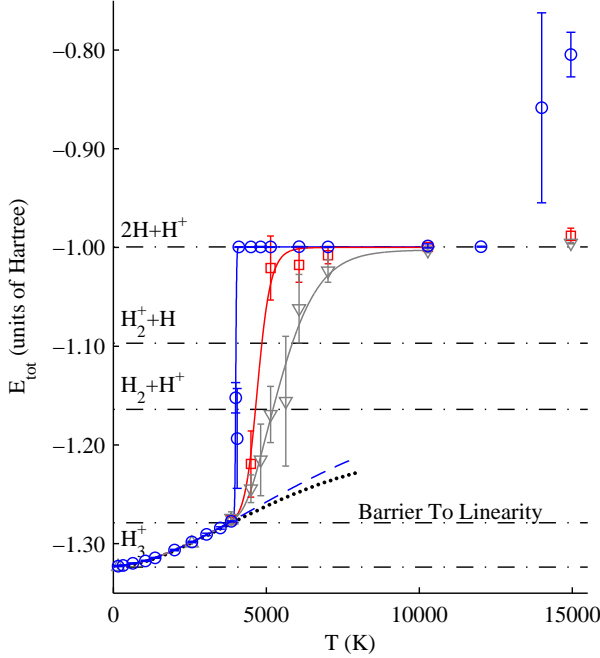


FIG. 1.— (Color online) NVT total energy of the H_3^+ molecular ion as a function of temperature at three different densities: blue circles ($\sim 1.255 \times 10^{-6} \text{ g cm}^{-3}$), red squares ($\sim 3.388 \times 10^{-5} \text{ g cm}^{-3}$) and gray triangles ($\sim 2.710 \times 10^{-4} \text{ g cm}^{-3}$). The blue dashed line is the energy fitted to Eq. (7). The black dots give the energy computed using the partition function fit given by Neale and Tennyson (1995). The horizontal dash-dotted lines are the nonadiabatic zero Kelvin energies for the ion, its fragments and the barrier to linearity. The high temperature solid lines are mainly for guiding the eye, but used for numerical evaluation of the partition function, later.

to the energy. However, it is worth pointing out that the temperature limits of these three ranges, i.e. 0 – 4000 K, 4000 – 10000 K and above 10000 K, are subject to changes with larger variation of densities.

Above 10000 K in our lowest density case the thermal ionization of H atoms is evident, see Fig. 1, but for our higher density cases some 15000 K is needed to show first signs of ionization. Similar trend for the ionization is stated in Koskinen *et al.* (2010), although there the density is notably less than our lowest one.

Let us now consider the dissociation recombination reaction chain, Eq. (2), and the contributing fragments to the quantum statistical NVT equilibrium trying to give an intuitive classical-like picture of the composition. With finite T , instead of zero, we have finite β , instead of infinite, that brings classical nature to the system the more, the higher the temperature. In other words, the partial decoherence in our five particle quantum system increases with increasing temperature, that enables us to distinguish the fragments as separate molecules and atoms in thermal equilibrium. Based on this interpretation, we show the total energy distribution in Fig. 2 from sampling the imaginary time paths at about 5000 K with $M = 2048$ in our highest simulation density.

We see three main peaks and by inspection of the energy distribution the first and the second can clearly be assigned to the rovibrationally excited H_3^+ and H_2+H^+ , respectively. As expected, there are no rovibrational excitations available for $2\text{H}+\text{H}^+$, leading to the peak average position very close to $-1E_{\text{H}}$. The fourth fragment,

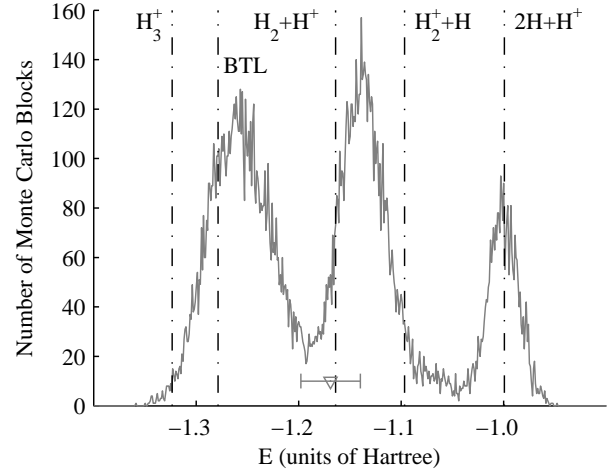


FIG. 2.— (Color online) Histogram of total energy sampling pinned in boxes of width $0.001E_{\text{H}}$ from $(2 \times 10^4) \times 10^5$ Monte Carlo samples averaged over blocks of 10^5 samples. The simulation density, temperature and Trotter number are $\sim 2.710 \times 10^{-4} \text{ g cm}^{-3}$, $\sim 5139.6 \text{ K}$ and 2048, respectively. Other notations are taken from Fig. 1.

H_2^++H , can be identified as the small high-energy side shoulder of H_2+H^+ peak. With the interpretation of the area under the peak as the abundance of the fragment in the equilibrium we find this contribution to be much smaller than that of the others.

It is important to note, however, that the above illustration is dependent on the block averaging procedure, see the caption of Fig. 2. Pinning the energy data of each and every sample, i.e. choosing block of size one sample, would broaden the peaks in Fig. 2. At the opposite limit, all samples in one block, the single mean energy or ensemble average is the quantum statistical expectation value $-1.169(29)E_{\text{H}}$, see Table 2, Figs. 1 and 2, where the statistical uncertainty decreases with increasing simulation length.

3.2. Molecular partition function

To compare with the other published approaches for the molecular partition function based on single molecule quantum chemistry we start from the lowest temperature range from 0 to $\sim 4000 \text{ K}$, where the molecule does not essentially dissociate, yet.

We present a low temperature H_3^+ molecular partition function as a first approximation for the modeling of low density H_3^+ ion containing atmospheres. Our aim is to find a simple analytical form, which can be accurately fitted to the NVT energies from our simulations.

The partition function in terms of the Helmholtz free energy F is written as

$$Z = e^{-\beta F}, \quad (3)$$

where $\beta = (k_{\text{B}}T)^{-1}$, and the energy expectation value is straightforwardly derived from the partition function as

$$\langle E \rangle = -\frac{1}{Z} \frac{\partial Z}{\partial \beta}. \quad (4)$$

After solving the free energy from Eq. (3) as

$$F(T) = -k_{\text{B}}T \ln Z(T) \quad (5)$$

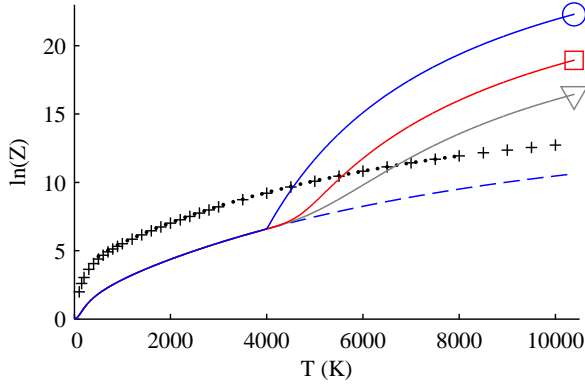


FIG. 3.— (Color online) The molecular NVT ensemble $\ln Z(T)$ from the energetics in Fig. 1 with the same notations. The blue solid line below 4000 K and its extrapolation (dashed line) are from Eq. (8), whereas the curves for three densities are from Eq. (9). The black data (points) and fit (pluses) of Neale and Tennyson (1995) are also shown.

we write $F(T) = -k_B T f(T)$ and the energy expectation value may be written as

$$\langle E \rangle = k_B T^2 \frac{\partial f(T)}{\partial T}. \quad (6)$$

We find that a well-behaving function fitting perfectly into our simulation data,

$$\langle E \rangle = k_B T^2 (a e^{-bT} + c) + d e^{-\alpha/T}, \quad (7)$$

allows analytical integration of Eq. (6) for $f(T)$ or $\ln Z(T)$,

$$\ln Z(T) = -\frac{a}{b} e^{-bT} + cT + \frac{d}{k_B \alpha} e^{-\alpha/T} + D. \quad (8)$$

Using the boundary condition for the molecular partition function with a nondegenerate ground state, $Z(0) = 1$ or $\ln Z(0) = 0$, we get $D = a/b$ in our model. However, inclusion of the contributions from the ground state spin degeneracy factor and the zero-point rotations would give $Z(0) = \xi > 1$, which would lead to $D = a/b + \ln \xi$, and thus, shift the function $\ln Z$ by a constant, only.

The weighted least squares fit of the above energy function, Eq. (7), to our data for temperatures up to about 3900 K, see Table 1, gives the parameters

$$\begin{aligned} a &= 0.00157426 \\ b &= 0.000132273 \\ c &= -6.15622 \times 10^{-6} \\ d &= 0.00157430 \\ \alpha &= 269.410 \\ D &= a/b \approx 11.9016. \end{aligned}$$

In the fit, in addition to the $(2\text{SEM})^{-2}$ weights, we force the first derivative of the energy with respect to the temperature to be monotonically increasing up to 3900 K. The fit extrapolates the 0 K energy to about $0.000549 E_H$ above that of the para- H_3^+ , i.e. it gives an excellent match within the statistical error estimate.

In Fig. 3 the function $\ln Z(T)$ from Eq. (8) is shown in the range $0 < T < 4000$ K — the behaviour of the model at higher T is illustrated by the dashed line. Above 4000 K the three curves for different densities are obtained

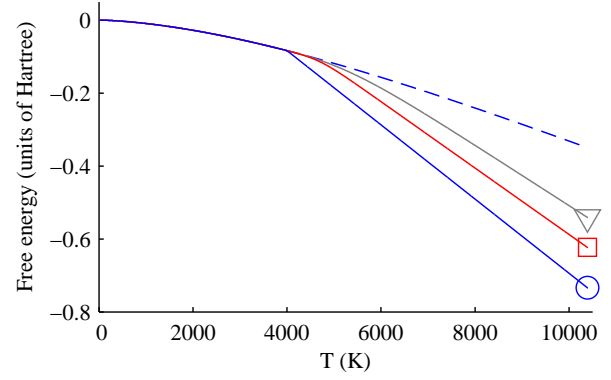


FIG. 4.— (Color online) Helmholtz free energy from Eq. (5) (in units of Hartree). Notations are the same as in Fig. 3.

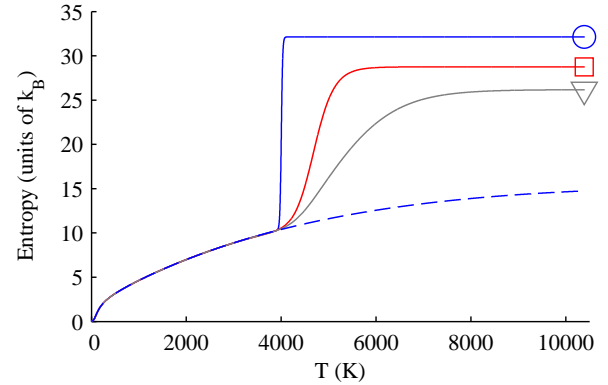


FIG. 5.— (Color online) Entropy from Eq. (10) (in units of k_B). Notations are the same as in Fig. 3.

from those shown in Fig. 1 by numerical integration of Eq. (6) as

$$\ln Z(T) = \ln Z(T_1) + \int_{T_1}^T \frac{\langle E \rangle}{k_B T^2} dT, \quad (9)$$

where $T_1 = 500$ K.

Neale and Tennyson (1995) have presented the partition function $\ln Z(T)$ based on a semi-empirical potential energy surface, see Fig. 3. The overall shape is similar to the one of ours. However, the energy $\langle E \rangle$ evaluated from their fit tends to be systematically lower than ours, although roughly within our 2 SEM error limits. Thus, the deviations are not visible in Fig. 1. For the partition function the main difference is in their zero reference, which also leads to $\ln \xi = -\infty$. This difference in zero reference goes back to that of energetics: our $\langle E \rangle$ in Eq. (7) at $T = 0$ fits perfectly the zero Kelvin energy of para- H_3^+ , as mentioned earlier. The zero Kelvin energy of the Neale and Tennyson (1995) behind their partition function is that of the spin forbidden $J = 0$ state, i.e. $Z(0) = 0$. This in fact, leads to the divergence of $\ln Z(T)$ at $T = 0$.

Our low temperature partition function Eq. (8) is close to complete. With the PIMC approach we implicitly include all of the quantum states in the system with correct weight without any approximations. This partition function is the best one for the modeling of the low density H_3^+ ion containing atmospheres, at the moment. However, it is valid up to about 4000 K, only. As soon as

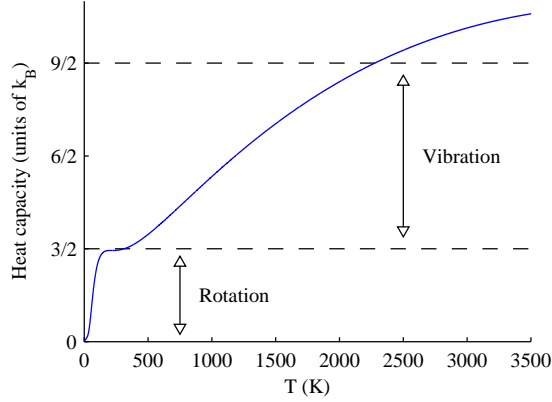


FIG. 6.— (Color online) Heat capacity as a function of temperature calculated using the analytical model of this work. The values on the y-axis are given in units of the Boltzmann constant k_B .

the density dependence starts playing larger role more complex models are needed. Such models can be fitted to our PIMC data given in Tables 1 and 2.

3.3. Other thermodynamic functions

In Fig. 4 we show the Helmholtz free energy from Eqs. (5) and (8), combined. As expected, lower density or larger volume per molecule lowers the free energy due to the increasing entropic factor. Dissociation and the consequent fragments help in filling both the space and phase space more uniformly or in less localized manner.

This kind of decreasing order is seen more clearly in the increasing entropy, shown in Fig. 5. The entropy has been evaluated from

$$S = \frac{U - F}{T}, \quad (10)$$

where the internal energy is $U = \langle E \rangle - \langle E \rangle_{T=0}$. As expected, both the total energy (internal energy) and entropy reveal the dissociation similarly.

Finally, in Fig. 6 we present the heat capacity

$$C_V = \frac{\partial \langle E \rangle}{\partial T}, \quad (11)$$

where $\langle E \rangle$ is taken from Eq. (7), which is valid at low temperatures, only.

Considering the goodness of our functional form for $\langle E \rangle$, it is very convincing to see the plateau at about $3/2 k_B$ corresponding to "saturation" of the contribution from the three rotational degrees of freedom. Thus, above 200 K the rotational degrees of freedom obey the classical equipartition principle of energy. It is the last term in the functional form of Eq. (7), that gives the flexibility for such detailed description of the energetics.

It should be emphasized that the plateau is not artificially constructed to appear at $3/2 k_B$, except for a restriction given for the first derivative of the total energy to be increasing. Thus, the analytical model we present, Eq. (7), is found to be exceptionally successful at low temperatures.

4. CONCLUSIONS

We have evaluated the temperature dependent quantum statistics of the five particle molecular ion H_3^+ far

TABLE 1
NVT ENERGETICS OF THE H_3^+ MOLECULAR ION AT LOW TEMPERATURES — HERE THE SAME DATA APPLIES FOR ALL THREE DENSITIES. THE ENERGIES ARE GIVEN IN THE UNITS OF HARTREE (ATOMIC UNITS) AND WITH 2 SEM ERROR ESTIMATES. THE ENERGIES FROM OUR LOW T FIT (LTFIT) FROM EQ. (7) AND THOSE FROM THE FIT OF NEALE AND TENNYSON (1995) (NT) ARE ALSO GIVEN AS COMPARISON. AT 0 K THE BEST UPPER BOUND IS GIVEN, SEE THE FOOTNOTE^c.

$T(K)$	PIMC ^a	LTFIT ^a	NT fit ^b
0		-1.3231	(-1.32367) ^c
~ 160.61	-1.3227(7)	-1.3227	-1.3232
~ 321.22	-1.3221(6)	-1.3220	-1.3225
~ 642.45	-1.3198(6)	-1.3202	-1.3209
~ 1052.6	-1.3173(7)	-1.3171	-1.3179
~ 1365.2	-1.3143(5)	-1.3141	-1.3148
~ 2000.3	-1.3064(7)	-1.3065	-1.3070
~ 2569.8	-1.2983(8)	-1.2984	-1.2989
~ 3049.2	-1.2905(12)	-1.2909	-1.2917
~ 3499.3	-1.2840(12)	-1.2835	-1.2847
~ 3855.6	-1.2774(7)	-1.2774	-1.2792

^aThis work.

^bCalculated from the fit given in Neale and Tennyson (1995).

^cPara- H_3^+ , see refs. Kutzelnigg and Jaquet (2006) and Pavanello and Adamowicz (2009).

TABLE 2
PIMC NVT ENERGETICS OF THE H_3^+ MOLECULAR ION AT HIGH TEMPERATURES FOR THE THREE DENSITIES (EXPRESSED AS THE NUMBER OF MOLECULAR IONS PER VOLUME), SEE FIG. 1. NOTATIONS ARE THE SAME AS IN TABLE 2.

$T(K)$	$(300a_0)^{-3}$	$(100a_0)^{-3}$	$(50a_0)^{-3}$
~ 3999.2	-1.152(16)		
~ 4050.0	-1.19(6)		
~ 4100.4	-0.9995(4)		
~ 4498.2	-0.9993(4)	-1.219(34)	-1.244(15)
~ 4819.5	-0.9993(4)		-1.215(37)
~ 5139.6	-0.9995(4)	-1.020(33)	-1.169(29)
~ 5634.8			-1.156(66)
~ 6070.3	-0.9991(4)	-1.018(18)	-1.062(35)
~ 7017.2	-0.9995(4)	-1.008(9)	-1.024(12)
~ 10279	-0.997(3)	-0.9995(8)	-1.003(3)
~ 12016	-0.9993(6)		
~ 13997	-0.86(10)		
~ 14951	-0.805(23)	-0.988(8)	-0.9957(8)

beyond its dissociation temperature at about 4000 K. This is done with the path integral Monte Carlo (PIMC) method, which is basis set and trial wave function free approach and includes the Coulomb interactions exactly. Thus, we are able to extend the traditional *ab initio* quantum chemistry with full account of correlations to finite temperatures without any approximations, also including the nuclear thermal and quantum dynamics.

It is fair to admit, however, that PIMC is computationally heavy for good statistical accuracy and approximations are needed to solve the "Fermion sign problem" in cases where exchange interaction becomes essential.

The temperature dependent mixed state description of the H_3^+ ion, the density dependent equilibrium dissociation recombination balance and the energetics has been evaluated for the first time. With the rising temperature the rovibrational excitations contribute to the energetics, as expected, whereas the electronic part remains in

its ground state in the spirit of the Born–Oppenheimer approximation. At about 4000 K the fragments of the molecule, $\text{H}_2 + \text{H}^+$, $\text{H}_2^+ + \text{H}$ and $2\text{H} + \text{H}^+$, start contributing. Therefore, H_3^+ ion becomes less dominant, and eventually negligible in high enough T .

We have shown how the partial decoherence in the mixed state can be used for interpretation of the fragment composition of the equilibrium reaction. Furthermore, we have evaluated explicitly the related partition function, free energy, entropy and heat capacity, all as functions of temperature. An accurate analytical func-

tional forms are given for the temperatures below dissociation. We consider all these as major improvements to the earlier published studies, where dissociation has not been considered.

5. ACKNOWLEDGEMENTS

For financial support we thank the Academy of Finland, and for computational resources the facilities of Finnish IT Center for Science (CSC) and Material Sciences National Grid Infrastructure (M-grid, akaatti).

REFERENCES

- Ceperley, D. M. 1995, *Rev. Mod. Phys.*, 67, 279
 Chakravarty, C., Gordillo, M. C., and Ceperley, D. M. 1998, *J. Chem. Phys.*, 109, 2123
 Cuervo, J. E. and Roy, P.-N. 2006, *J. Chem. Phys.*, 125, 124314
 Dinelli, B. M., Polyansky, O. L., and Tennyson, J. 1995, *J. Chem. Phys.*, 103, 10433
 Feynman, R. P. 1998, *Statistical Mechanics*, Perseus Books, Reading, Massachusetts
 Harris, G. J., Lynas-Gray, A. E., Miller, S., and Tennyson, J. 2004, *ApJ*, 600, 1025
 Herman, M. F., Bruskin, E. J., and Berne, B. J. 1982, *J. Chem. Phys.*, 76, 5150
 Knoll, L. and Marx, D. 2000, *Europ. Phys. J. D*, 10, 353
 Koskinen, T. T., Aylward, A. D., and Miller, S. 2009, *Astrophys. J.*, 693, 868
 Koskinen, T. T., Aylward, A. D., Smith, C. G. A., and Miller, S. 2007, *ApJ*, 661, 515
 Koskinen, T. T., Yelle, R. V., Lavvas, P., and Lewis, N. K. 2010, *ApJ*, 723, 116
 Kutzelnigg, W. and Jaquet, R. 2006, *Phil. Trans. R. Soc. A*, 364, 2855
 Kwon, Y. and Whaley, K. B. 1999, *Phys. Rev. Lett.*, 83, 4108
 Kylänpää, I. and Rantala, T. T. 2009, *Phys. Rev. A*, 80, 024504
 Kylänpää, I. and Rantala, T. T. 2010, *J. Chem. Phys.*, 133, 044312
 Lystrup, M. B., Miller, S., Russo, N. D., R. J. Vervack, J., and Stallard, T. 2008, *ApJ*, 677, 790
 Metropolis, N., Rosenbluth, A. W., Rosenbluth, M. N., Teller, A. H., and Teller, E. 1953, *J. Chem. Phys.*, 21, 1087
 Neale, L., Miller, S., and Tennyson, J. 1996, *ApJ*, 464, 516
 Neale, L. and Tennyson, J. 1995, *ApJ*, 454, L169
 Pavanello, M. and Adamowicz, L. 2009, *J. Chem. Phys.*, 130, 034104
 Pierce, M. and Manousakis, E. 1999, *Phys. Rev. B*, 59, 3802
 Storer, R. G. 1968, *J. Math. Phys.*, 9, 964
 Thomson, J. J. 1911, *Philos. Mag.*, 21, 225